2011 IEEE/ASME International Conference on
Advanced Intelligent Mechatronics (AIM2011)
Budapest, Hungary, July 3-7, 2011

Infrared Sensor Based Target Following Device for a Mobile Robot

Youg Jen Wen, Chia-Hung Tsai, Wei-Shun Yu, and Pei-Chun Lin

Abstract—**A sensory setup and algorithm for target following on the mobile robot is reported. The target detection, including its direction and distance, is achieved by the low-cost infrared transmitter and receiver pair. The transmitted signal is coded so the receiver is free from environmental disturbances. The motion of the follower has obstacle avoidance capability achieved by utilizing an ultrasonic sensor array. The proposed algorithm derives the follower locomotion by adequately fusing the information from both sensor modules. Experimental validation is executed to evaluate the performance the proposed device.**

I. Introduction

The fast development of the robotics in recent years brings up several new issues regarding the human robot interaction (HRI). How to design a robot which can perform variety of tasks and in the meantime adequately serve and accompany with human in the human environment gradually becomes an important task. Among them, design a mobile platform which can follow the human locomotion is one of the popular topics. In order to achieve this goal, the follower should be capable of detecting the direction and distance from the target, and then it should be capable of moving effectively and safely without any collision with obstacles, thus to follow the target successfully.

Several methods can achieve the target detection or following, and vision is one of the popular methods. For example, using single camera to catch the leg motion of the human target [1], using single camera to catch the infrared signals transmitted from the target [2], using stereo vision to identify the target and obstacle [3], etc. Target tracking achieved by infrared (IR) transmitter and receiver pairs together with fuzzy logic was reported [4]. Inertial sensors was also utilized to compute the target speed and orientation [5]. RFID was adopted to track target by the intensity RF information [6]. In order to get precise motion information, the algorithm which is capable of recognizing people intention by using laser range finder (LRF) was reported [7]. LRF in general is a sensor with high precision, wide detection range, and high reliability. In addition, human tracking by utilizing multiple sensors with fusion scheme was reported as well. For example, fusion of the signals from LRF and vision sensor [8] or fusion of infrared sensors and sonar [9] to track the target. The successful target tracking includes two subtasks: one is detect the target, and the other one is to perform the adequate locomotion. For the latter one, obstacle avoidance in most scenarios is necessary [10], and the potential field method is also widely adopted, where the follower was "attracted" to the target and was "pushed away" from the obstacles [11].

Here, we report on the low-cost sensory setup and algorithm for the target following on the mobile robot. The target detection, including its direction and distance, is achieved by the low-cost IR transmitter and receiver pair. The transmitted signals are coded so the receiver is free from environmental disturbances. Comparing to the conventional vision method, this method avoids the necessity of pre-process of learning the target motion as well as has the advantage of low computation power and high sensor sampling rate. The target can be followed as long as the transmitter is carried. The motion of the follower has obstacle avoidance capability achieved by utilizing an ultrasonic sensor array. The proposed algorithm derives the follower locomotion by adequately fusing the information from both sensor modules.

The paper is organized as follows: Section II describes the design of the target detection module. Section III presents the algorithm of target following with obstacle avoidance. Section IV presents the generation of the follower locomotion, and Section V presents the experimental evaluation. Section VI concludes the work.

II. Design of the Target Detection Module

In order to achieve the target following task, it is necessary for the follower to know the relative position between the target and itself. This information includes two states, the direction and the distance, and more specifically, the position of the target can be represented in the polar coordinates of the coordinate system built on the follower, (θ_o, ℓ_o). In addition, assume that $\theta=0$ represents the nominal heading of the follower.

The IR transmitter and receiver are chosen to achieve the direction detection of the target θ_o because the IR light in principle is directional and invisible by the human. The former one and latter one are installed on the target and the follower, respectively. Since the device is intended to be used in the normal environment where lots of other infrared signals may exist, the signal exchanged between the transmitter and receiver are coded according to a specific protocol, which in empirical is done by a commercial transmitter-receiver IC pair. In addition, though the IR light signal itself is directional, the commercial IR receivers are usually designed to be capable of receiving the IR signals from a wide range of directions. Thus, to prevent IR receiver receiving the IR signal from unwanted directions, a custom design of the housing of the IR receiver is required.

Several experimental tests were performed to evaluate the directional effect of the IR receiver. As shown in Fig 1(a)

This work is supported by National Science Council (NSC), Taiwan, under contract 99-2218-E-002-012-.

Authors are with Department of Mechanical Engineering, National Taiwan University (NTU), No.1 Roosevelt Rd. Sec.4, Taipei 106, Taiwan. (Corresponding email: peichunlin@ntu.edu.tw).

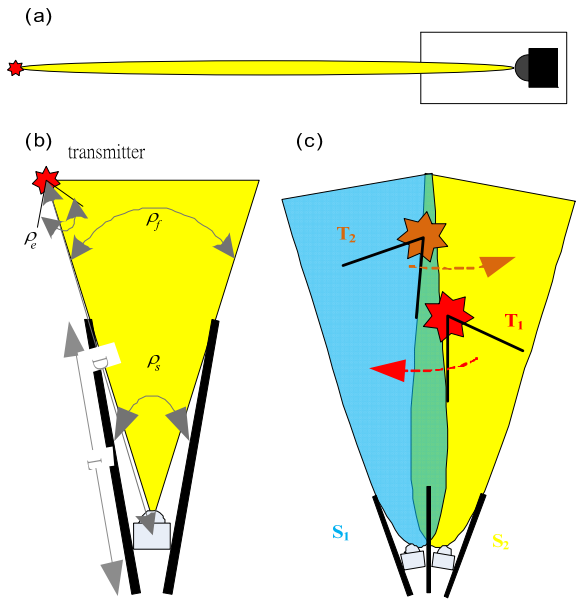

Fig. 1. (a) IR transmitter (red star) and receiver (black shape) pair; (b) the single unit test, including the definition of the terminologies; (c) actual detectable area of each unit (blue or yellow region).

where the IR receiver is installed inside a black hollow cylinder, experimental result shows that the IR receiver can receive the signal emitted from the IR transmitter only when the transmitter is placed in front and along with the axis of the cylinder, which confirms the directional property of the light. Because of this confirmed characteristic, the detection range of the receiver can be adjusted by placing the side walls around the receiver. One of the simplest methods to deploy several receivers to cover the front 180-degree detection range is to equally divide the detection range by the number of the utilized receivers, just like slicing the cake shown in Fig 2(a).

In order to evaluate the performance of each "sliced" sensor unit, the experimental setup shown in Fig 1(b) is built to evaluate the effect of length of the side wall L and designed detection angle ρ_s to the actual detectable angle, ρ_f. The results listed in Table I reveal that with the same length of the side wall, the actual detectable angle ρ_f is larger than the designed detection angle ρ_s while the distance between the transmitter and the receiver, D, is short, and the former one ρ_f approaches the latter one ρ_s while D increases. This phenomenon is mainly due to the fact that for a small distance D, the intensity of the reflected incoming IR signal from the side wall is still strong enough to trigger the receiver. Thus, even when the transmitter is not located within the designed detection angle ρ_s, the receiver is still capable of sensing the signal from it. When the distance D increases, the intensity of the incoming signal has already been weaken due to long travel distance, so only the direct-incoming signal without any reflection can trigger the receiver. Therefore, the designed detection angle and the actual detectable angle can be treated equal in this case. In an effort to remedy the effect of light reflection, the black smooth acrylic is adopted as the side walls, which has the larger light absorption rate and less light scattering effect. On the transmitter side, each

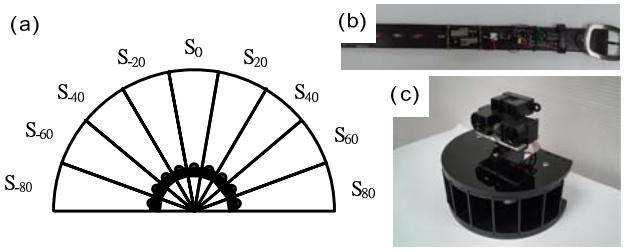

Fig. 2. (a) Configuration of nine IR receivers installed inside the semicircle-shape housing; (b) photo of the belt with transmitters wear by the target; (c) photo of the target detection device.

TABLE I Actual detectable angle versus designed detection angel under various settings

L=10 cm			
	D=1m	*D=3m*	*D=5m*
ρ_s=45°	ρ_f=63°	ρ_f=57°	ρ_f=49°
ρ_s=30°	ρ_f=44°	ρ_f=40°	ρ_f=34°
ρ_s=20°	ρ_f=34°	ρ_f=30°	ρ_f=24°
L=7.5 cm			
	D=1m	*D=3m*	*D=5m*
ρ_s=45°	ρ_f=64°	ρ_f=58°	ρ_f=49°
ρ_s=30°	ρ_f=45°	ρ_f=40°	ρ_f=34°
ρ_s=20°	ρ_f=35°	ρ_f=30°	ρ_f=24°
L=5 cm			
	D=1m	*D=3m*	*D=5m*
ρ_s=45°	ρ_f=73°	ρ_f=62°	ρ_f=52°
ρ_s=30°	ρ_f=54°	ρ_f=45°	ρ_f=36°
ρ_s=20°	ρ_f=38°	ρ_f=32°	ρ_f=26°

transmitter also has certain emitting angle ρ_f. Empirical test confirms that the receiver can be triggered as long as the emitting directions of the transmitter and the detectable directions of the receiver has certain overlap as shown in Fig 2(c). Table also reveals that the lengths of the side wall L equaled to *7.5* and *10* cm have similar effect on the actual detectable angle ρ_f, and ρ_fs of those both cases have faster converging rate to ρ_s than that of L equaled to *5*cm. This is reasonable since the filtering of the unwanted incoming light is better when the length of the side wall increases. Once the length of L passes certain threshold where the intensity of the reflected incoming signal can never trigger the receiver, the further increase of L has insignificant effect.

The blue and yellow areas shown in Fig 1(c) depict the detectable ranges of the receiver S_1 and S_2, respectively. The configuration of the transmitter T_1 indicates the right limit of the transmitter which can be sensed by the receiver S_1. The S_1 can sense T_1 adequately if the T_1 moves left or orients toward left. Similarly, the configuration of the transmitter T_2 indicates the left limit of the transmitter which can be sensed by the receiver S_2. The transmitter placed in the blue or yellow region with adequate emitting angle can be sensed by

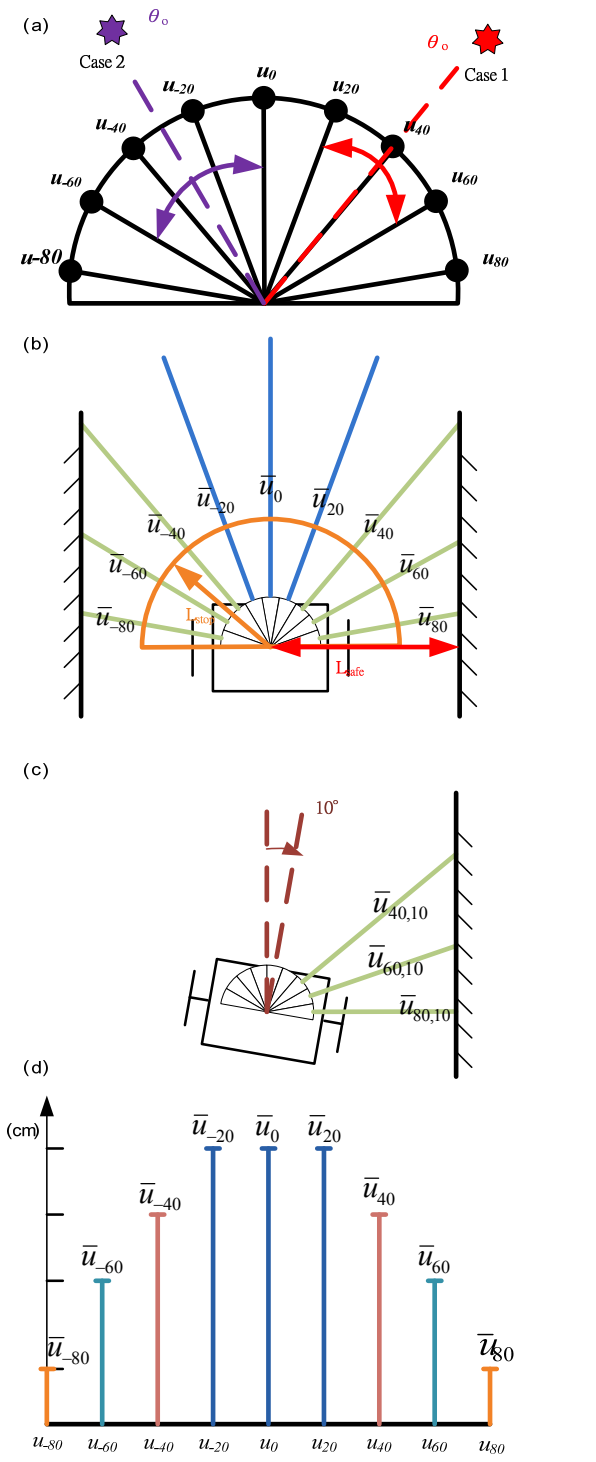

Fig. 3. (a) Configuration of nine ultrasonic range finders installed on the follower; (b) the configuration where the thresholds $\bar{u}_j$ are set up; (c) the configuration where the thresholds $\bar{u}_{j,10}$ are determined; (d) the values of the thresholds $\bar{u}_j$.

only one receiver. However, if the transmitter is placed in the green region, both receivers can sense the transmitter.

In the final design, a bank of nine receivers is adopted to cover the front 180-degree detection range, so the designed detection angle of each receiver ρ_s is 20 degree. In addition, *L=5cm* is chosen for its compact size. Because the actual detectable angle ρ_f in *L=5cm* case is larger than that in *L=7.5cm* or *10cm* case, the overlapped green area is larger as well. The reasonably increase of the overlapped region improves the resolution of the direction detection. For example, for the same distance *D*, if the arc in the green region is equal to that in the yellow or blue region, the resolution increases to 10 degree. If there is no overlapped green region, the resolution is 20 degree, equaling to the designed detection angle. Because the actual detectable angle ρ_e varies with the distance *D*, the resolution of the direction detection is a function of the distance between the transmitter and the receiver *D*, within the range 10-20 degree. In current design at most two receivers can sense the transmitter simultaneously.

Assuming there is no obstacle impeding the light travel from the transmitter to the receiver, the direction of the target θ_o can be represented as:

$$\theta_o = \frac{\sum_i i\, S_i}{\sum_i S_i}, \quad (1)$$

where $i = [80 \;\; 60 \;\; 40 \;\; 20 \;\; 0 \;\; -20 \;\; -40 \;\; -60 \;\; -80]$, representing the physical directional in degree, and

$$S_i = \begin{cases} 1 & triggered \\ 0 & else \end{cases}.$$

Though 9 terms are summed up in (1), please remind that at most two S_is are 1 (i.e., receiver triggered), and the others are 0.

The IR distance sensor installed on a small RC servo motor is chosen to achieve the distance detection between the target and the follower. After the follower knows the direction of the target θ_o, the RC servo quickly rotates the IR distance sensor to aim at that direction, so the distance between the target and the follower, ℓ_o, can be obtained. If the side moving of the target is slow (i.e., θ_o changes slowly), the RC servo may not be necessary, and the equivalent rotation can be achieved by the motion of the follower. However, in general the turning response of the follower itself is slower than the side motion of the target. In addition, by turning the RC rather than the follower to obtain distance detection can avoid the follower performing high frequency rotation motion, so the follower can move in a smooth trajectory.

In summary, the state of the target relative to the follower, (θ_o, ℓ_o), are obtained according to the algorithm described in this section. Next, the question lies in how to generate adequate motion of the follower to follow the target.

III. TARGET FOLLOWING WITH OBSTACLE AVOIDANCE

If the follower tails the target very closely, the motion of the follower can be programmed to follow the "movable" target point, and the obstacle avoidance capability in the follower is not necessary, as long as the target can avoid the obstacles successfully. However, in general following tasks where certain distance exists between the target and the follower, the capability of performing the obstacle avoidance in the follower is crucial. For example, if the task is human following, the comfortable distance for human to be tailed is at least 1 meter, and it is hard to guarantee that the space between the human and the follower is clear at all time. Thus, in this section the motion of the follower with obstacle avoidance capability is described.

Nine ultrasonic range finders are installed on the follower to cover the front 180-degree environment sensing capability as shown in Fig. 3(a). The installation and alignment of the ultrasonic range finders are similar to that of the IR receivers, equally distributed on the semicircle. Thus, the difference of the sensing direction between the consecutive sensors is 20 degree. The ultrasonic range finder itself has ~45 degree receiving cone, so in current arrangement the sensing areas have some overlap to make sure the front area are sensed thoroughly. Assume u_j is the distance of the obstacle measured by the sensor, where the notation of $j = [80\ \ 60\ \ 40\ \ 20\ \ 0\ \ -20\ \ -40\ \ -60\ \ -80]$, similar to the definition of the IR receivers shown in the previous section.

Nine threshold $\bar{u}_j$s are defined as the safety measure of the follower's motion. Because the follower faces the target most of the time, the defined thresholds of the six range finders on both sides are mainly determined by the geometrical configuration of the follower relative to the imaginary side wall as shown in Fig 3(b). Here L_{safe} is set to 55cm and the $\bar{u}_j$s are calculated as $\bar{u}_j = L_{safe}/\cos(90 - \text{abs(j)})$, where $j = \pm 40, \pm 60 \pm 80$. The $\bar{u}_j$s of the three front sensors are set as the judgment whether the follower can go forward or not because the combined sensed range is wider than the width of the follower. Empirically the value is set as $\bar{u}_j = 75$ cm, $j = 0, \pm 20$. In addition, when the sensed u_j is less than $L_{stop} = 37.5\text{cm}$, the follower stops immediately to avoid any potential collision.

A function $f_j(u_j)$ is defined to represent the obstacle status around the follower:

$$f_j(u_j) = \begin{cases} 1 & if\ u_j \le \bar{u}_j \\ 0 & else \end{cases},$$

where the value 1 indicates that the robot is too close to the obstacle in the *j* direction. The value 0 indicates no obstacle in that direction. In addition, the follower can move in a specific direction safely if $f_j(u_j)$ in that direction and $f_j(u_j)$s of the consecutive right and left sensors are all 0. More specifically, three consecutive 0s are required for the follower to successfully move in that direction. Following that logic, the feasible following direction θ_b can be defined as

$$\begin{cases} \theta_b = \theta_o \quad if\ \sum_j f_j(u_j) = 0 \quad j = \theta_o, \theta_o \pm 20 \\ \theta_b = \tilde{\theta}_o\ if\ \sum_j f_j(u_j) = 0\ \ j = \tilde{\theta}_o, \tilde{\theta}_o \pm 20\ \ min\|\tilde{\theta}_o - \theta_o\| \end{cases},$$

if the direction of the target θ_o is derived to be the same as one of the number *j* (i.e., $\theta_o/10 \in$ even). If the derived θ_o is derived to be in between the number *j*s (ex, 10, 30, …), the criteria is

$$\begin{cases} \theta_b = \theta_o \quad if\ \sum_j f_j(u_j) = 0 \quad j = \theta_o \pm 10, \theta_o \pm 30 \\ \theta_b = \tilde{\theta}_o\ if\ \sum_j f_j(u_j) = 0\ \ j = \tilde{\theta}_o, \tilde{\theta}_o \pm 20\ \ min\|\tilde{\theta}_o - \theta_o\| \end{cases},$$

where obstacle status of 4 consecutive sensors is checked. In brief, if no obstacle in the θ_o direction, the follower moves toward that direction in order to follow the target adequately. If the obstacle exists, the follower will search for the suitable direction where (1) three consecutive $f_j(u_j)$s are 0s and (2) is as close to the θ_o as possible.

The algorithm shown above can effectively detour the path of the follower to avoid the obstacles in the original moving direction. However, the detoured path should also be checked with obstacle condition for safe follower motion. Thus, obstacle status sensed by six side sensors $f_j(u_j)$s is utilized to adjust the motion direction shown below:

$$\theta_s = \sum w_j \cdot f_j(u_j) \cdot \frac{u_j - \bar{u}_j}{\bar{u}_{j,10} - \bar{u}_j}, \quad j = \pm 40, \pm 60, \pm 80$$

where θ_s represents the direction adjustment, w_js indicate the weights of the sensor readings, and $\bar{u}_{j,10}$s are the constants calculated while the motion direction of the follower is 10 degree toward the side wall shown in Fig 3(c). Ten degree is chosen because the best resolution of direction θ_o is 10 degree. The direction adjustment is linearized and scaled according to this number.

Finally, the motion direction of the follower, θ_m, can be calculated as the linear combination of the above considerations:

$$\theta_m = \theta_b + \theta_s.$$

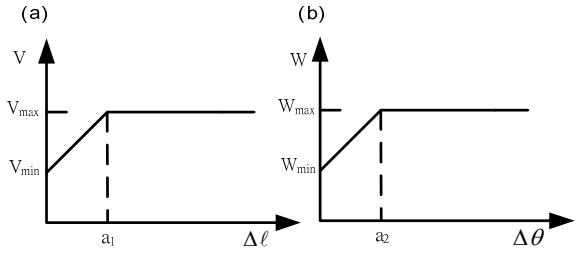

Fig. 4. The maximum forward speed (a) and turning speed (b) versus the errors of target tracking.

IV. Locomotion of the Follower

During the following motion, the follower is programmed to face the target directly and to follow the target with designate distance. Thus, with given (θ_o, ℓ_o) provided by the detection device described in Section II, the desired setting is $\theta_o^* = 0^o$ and $\ell_o^* = \text{constant}$, where the empirical value is set to 1 meter for human following. The control goal is to minimize the difference between the current value and the desired one:

$$\begin{cases} \Delta\theta = \theta_s - \theta_s^* \\ \Delta\ell = \ell_o - \ell_o^*. \end{cases}$$

The follower in general is a dynamic system which has certain response characteristic. One of the typical constraints is the maximum acceleration and deceleration the follower can achieve. Thus, in the empirical implementation the follower will accelerate and decelerate to minimize $\Delta\theta$ and $\Delta\ell$ in a constraint manner. For different desired distance ℓ_o^*s, the allowable speeds of the follower are also set to have different saturation values. The logic is similar to the car traveling in the highway where the higher speed requires the longer safety distance, so the response to any emergency is effective. In addition, the maximum allowable speed of the robot is set to 2 m/s for safety consideration.

The motion of the follower is basically followed speed control architecture, and the quantitative representation of the speed profile versus the $\Delta\ell$ and $\Delta\theta$ are shown in Fig 4 and listed as follows:

$$\begin{cases} V = \frac{V_{max} - V_{min}}{a_1}(\Delta\ell - a_1) & if\ \Delta\ell \le a_1 \\ V = V_{max} & else \end{cases},$$

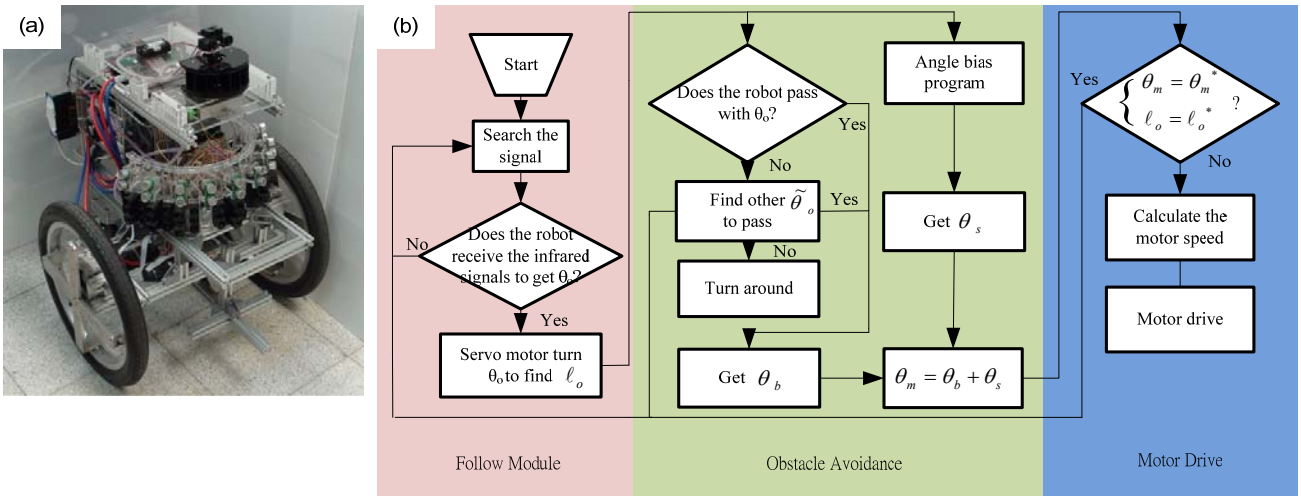

Fig. 5. (a) Photo of the follower utilized in the experimental validation; (b) The flowchart of the overall algorithm.

$$\begin{cases} W = \frac{W_{max}-W_{min}}{a_2}(\Delta\theta - a_2) & if\ \Delta\theta \le a_2 \\ W = W_{max} & else \end{cases},$$

where a_1 and a_2 are constants, and V and W represent forward and turning speeds, respectively. For the follower with two-wheel differential-drive mechanism, the speed can further be converted to the forward speeds of the left and right wheels (V_L and V_R),

$$\begin{cases} V = \frac{V_L+V_R}{2} \\ W = \frac{V_L-V_R}{b}, \end{cases}$$

where b is the distance between the wheels. The wheel rotation speeds can then be calculated as,

$$\begin{cases} \dot{\varphi}_L = \frac{V_L}{R} \\ \dot{\varphi}_R = \frac{V_R}{R}, \end{cases}$$

where R is the radius of the wheel.

V. Experimental Validation

The platform shown in Fig. 5(a) is utilized as the follower for experimental evaluation. A tester wearing the belt with transmitters shown in Fig. 2(b) acted as the target to be followed, so the following task is in certain level equals to the human following. The platform is a three-wheeled mobile robot with two-wheel differential drive as the actuating mechanism and a third wheel as an idler. Thus, it can perform 3 degree-of-freedom planar motion on the ground. The mechatronic system on the platform includes a detection device which senses the direction and distance of the target detailed in Section II, an ultrasonic sensor array to detect the surrounded obstacles, and a real time embedded control system (sbRIO-9642, National Instruments) which is in charge of algorithm computation and motion control. The overall logic flow chart is depicted in Fig. 5(b).

The proposed sensory setup and following algorithm were evaluated experimentally under various scenarios. A commercial HD camcorder (XDR-11, SONY) was placed on top of the scenarios to record the trajectories of the target and the follower. LEDs are installed on top of the target and the follower as the markers during the experiments, which ease the followed post processing in Matlab to extract the positions of the markers from a sequence of images. The results are shown in Fig 6, where the red line and blue line represent the trajectories of the target and follower, respectively. The same legends marked on two lines indicate the positions extracted from the same image, and this information provides the relative position between the target and the follower at several different time stamps.

Fig 6(a) and 6(b) plot the trajectories of the target and the follower while the target moves in a straight line and in a circular motion, respectively. The circular trajectory of the follower is smaller than that of the target because in the algorithm setting the follower moves toward the target, not to follow the exact trajectory of the target. Figure 6(c) and 6(d) plots the motion with a 90-degree turning, including inside and outside of a 'L' shape obstacle. With the obstacle avoidance setup, the follower chose the path closer to the wall but not bump into the wall even when the direction of the target is toward the wall. Figure 6(e) and 6(f) represents the trajectories of the target and the follower passing through a door, including two different configuration of the opened door. In both scenarios the follower can pass successfully. Figure 6(g) and 6(h) plots the motion through wide and narrow corridors, and Fig 6(i) plots the motion with two sharp turns in different directions. In summary, the experimental results shown in Fig 6 confirm that the proposed setup and algorithm is functional. In addition, in contrast to the human walking which has side swing motion, the robotic follower performs a smoother locomotion. The original movie clips can be found in the supplementary video.

VI. Conclusion

We report the sensory setup and algorithm for target following on the mobile robot. The direction detection of the target is achieved by the setup of nine IR receivers which monitor the signals from the transmitter installed on the target. Nine ultrasonic range finders are also installed on the follower to performance the obstacle avoidance task. The

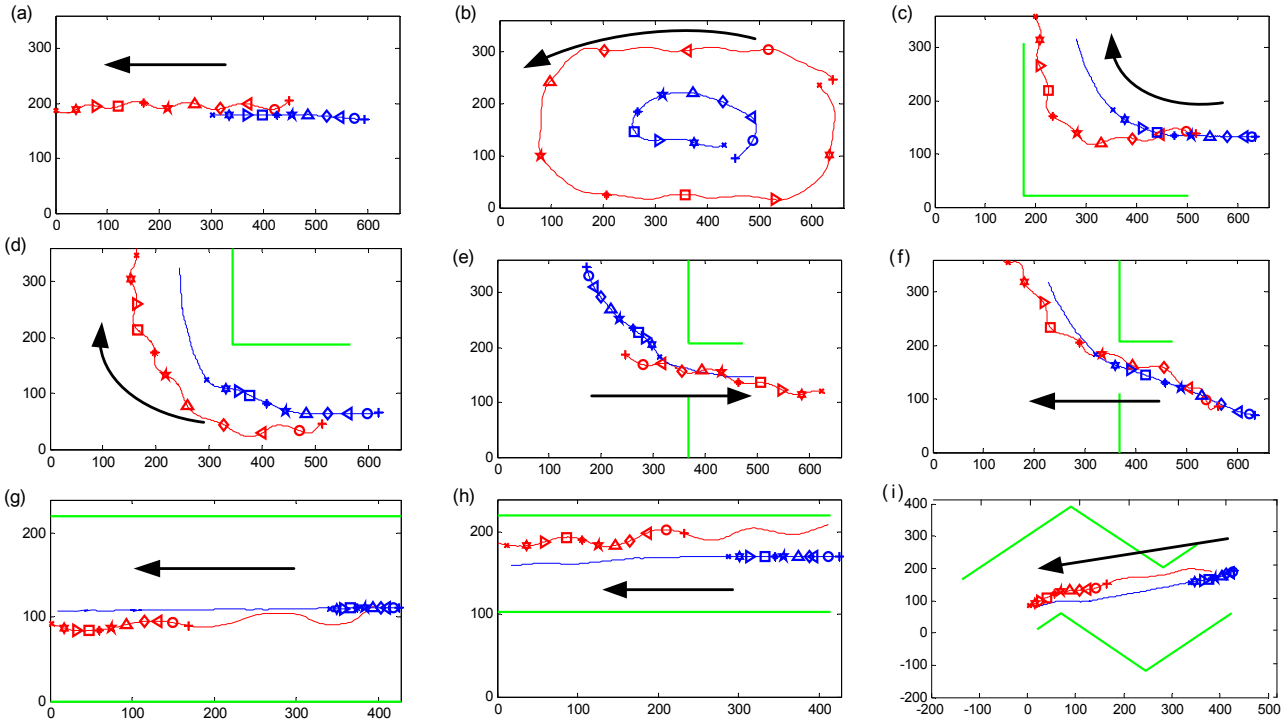

Fig. 6. Trajectories of the target (red line) and the follower (blue line) tested in various scenarios: (a) straight line motion; (b) circular motion; (c) inner right angle turn; (d) outer right angle turn; (e) door passing I; (f) door passing II. Black arrows indicate the direction of motion; (g) in wide corridor; (h) in narrow corridor; (i) S-shape motion. Black arrows indicate the direction of motion. Unit: cm.

proposed algorithm derives the follower locomotion by adequately fusing the information from both sensor modules. Experimental results show that the proposed method can successfully achieve target following in various scenarios, including straight line and circular motion, sharp-turn motion, door passing, corridor passing, and S-shape corridor following.

We are current in the process of developing a more sophisticate algorithm which can perform target following in a complicate and wide range of environment setup.

VII. Acknowledgment

The authors gratefully thank the National Instruments Taiwan Branch for their kindly support of equipments and technical consulting.

References

[1] N. Tsuda, *et al.*, "Mobile robot with following and returning mode," in *The 18th IEEE International Symposium on Robot and Human Interactive Communication (RO-MAN)* 2009, pp. 933-938.

[2] Y. Nagumo and A. Ohya, "Human following behavior of an autonomous mobile robot using light-emitting device," in *IEEE International Workshop on Robot and Human Interactive Communication (RO-MAN)* 2001, pp. 225-230.

[3] C.-H. Chao, *et al.*, "Real-time target tracking and obstacle avoidance for mobile robots using two cameras," in *ICROS-SICE International Joint Conference*, 2009, pp. 4347-4352.

[4] T. H. S. Li, *et al.*, "Fuzzy target tracking control of autonomous mobile robots by using infrared sensors," *Fuzzy Systems, IEEE Transactions on,* vol. 12, pp. 491-501, 2004.

[5] S. Bosch, *et al.*, "Follow me! mobile team coordination in wireless sensor and actuator networks," in *IEEE International Conference on Pervasive Computing and Communications (PerCom)* 2009, pp. 1-11.

[6] K. Myungsik, *et al.*, "RFID-enabled target tracking and following with a mobile robot using direction finding antennas," in *IEEE International Conference on Automation Science and Engineering (CASE)*, 2007, pp. 1014-1019.

[7] K. Seongyong and K. Dong-Soo, "Recognizing human intentional actions from the relative movements between human and robot," in *IEEE International Symposium on Robot and Human Interactive Communication (RO-MAN)* 2009, pp. 939-944.

[8] R. C. Luo, *et al.*, "Human tracking and following using sensor fusion approach for mobile assistive companion robot," in *Annual Conference of the IEEE Industrial Electronics Society (IECON)*, 2009, pp. 2235-2240.

[9] A. Korodi, *et al.*, "Aspects regarding the object following control procedure for wheeled mobile robots," *WSEAS Transactions on Systems and Control,* vol. 3, pp. 537-546, 2008.

[10] J. L. Martinez, *et al.*, "Object following and obstacle avoidance using a laser scanner in the outdoor mobile robot Auriga-alpha," in *IEEE/RSJ International Conference on Intelligent Robots and Systems (IROS)*, 1998, pp. 204-209 vol.1.

[11] L. Huang, "A potential field approach for controlling a mobile robot to track a moving target," in *IEEE International Symposium on Intelligent Control (ISIC)*, 2007, pp. 65-70.